A Letters Journal Exploring the Frontiers of Physics

May 2010

EPL, **90** (2010) 44001
doi: 10.1209/0295-5075/90/44001

www.epljournal.org

Scaling laws in turbulent Rayleigh-Bénard convection under different geometry

Hao Song and Penger Tong[a]

Department of Physics, Hong Kong University of Science and Technology - Clear Water Bay, Kowloon, Hong Kong

received 24 April 2010; accepted 12 May 2010
published online 28 May 2010

PACS 47.27.-i – Turbulent flows
PACS 44.25.+f – Natural convection
PACS 47.27.te – Turbulent convective heat transfer

Abstract – A systematic study of turbulent Rayleigh-Bénard convection is carried out in two horizontal cylindrical cells of different lengths filled with water. Global heat transport and local temperature and velocity measurements are made over varying Rayleigh numbers Ra. The scaling behavior of the measured Nusselt number $Nu(Ra)$ and the Reynolds number $Re(Ra)$ associated with the large-scale circulation remains the same as that in the upright cylinders. The scaling exponent for the rms value of local temperature fluctuations, however, is strongly influenced by the aspect ratio and shape of the convection cell. The experiment clearly reveals the important roles played by the cell geometry in determining the scaling properties of convective turbulence.

Introduction. – The discovery of scaling laws in the heat flux and temperature statistics [1] in turbulent Rayleigh-Bénard convection, where a fluid layer of thickness H is heated from below and cooled from the top, has stimulated considerable experimental and theoretical efforts [2–5], aimed at accurately determining and explaining the effective power laws of the global and local quantities in turbulent convection. Among them the global quantities include the Nusselt number $Nu(Ra, Pr)$, which is a normalized total heat flux, and the Reynolds number $Re(Ra, Pr)$ associated with the large-scale circulation speed U across the convection cell. There are two experimental control parameters in Rayleigh-Bénard convection. One is the Rayleigh number $Ra = \alpha g \Delta T H^3/(\nu\kappa)$, where g is the gravitational acceleration, ΔT is the temperature difference across the fluid layer, and α, ν, and κ are, respectively, the thermal expansion coefficient, the kinematic viscosity, and the thermal diffusivity of the convecting fluid. The other control parameter is the Prandtl number, which is defined as $Pr = \nu/\kappa$.

The theory of Grossmann and Lohse (GL) [3,6] explains the scaling behavior of $Nu(Ra, Pr)$ and $Re(Ra, Pr)$ by a decomposition of the thermal dissipation field $\epsilon_T(\mathbf{r})$ into two parts. In one scenario [3], $\epsilon_T(\mathbf{r})$ is decomposed into the boundary layer and bulk contributions, which have different scaling behavior with varying Ra and Pr. More recently, a second scenario was proposed [6] with $\epsilon_T(\mathbf{r})$ being decomposed into two different contributions: thermal plumes (including the boundary layers) and turbulent background. The latter scenario considered fluctuations in turbulent convection and gave predictions on the statistics of various local quantities, such as the rms value of local temperature fluctuations. While the two scenarios involve different physical pictures about the local dynamics of turbulent convection, the calculated scaling of $Nu(Ra, Pr)$ and $Re(Ra, Pr)$ using the two different models turns out to be of the same form. The GL theory is capable of providing a correct functional form of $Nu(Ra, Pr)$ and $Re(Ra, Pr)$ for a large number of transport and velocity measurements [1,7–18].

Up to now many of the convection experiments were conducted in upright cylindrical cells with the cylinder diameter D being comparable to its height H. These experiments have resulted in a large body of knowledge about the global heat transport [1,7–16], structure [17,18] and oscillations [18–21] of the large-scale circulation, boundary layer properties [22–25], local temperature [1,26] and velocity [18,27] fluctuations, structure and statistics of the local convective heat flux [28,29] and thermal dissipation rate [30,31]. Our current theoretical understanding of convective turbulence is largely built upon this body of experimental results [5,32].

While the use of small aspect-ratio cylinders has the advantages of simple cell geometry, better experimental

[a] E-mail: penger@ust.hk

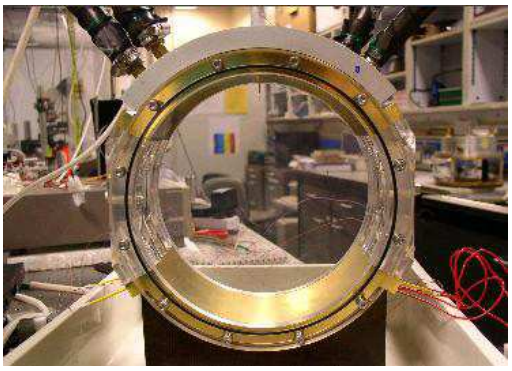

Fig. 1: (Colour on-line) Assembly of the horizontal convection cell. The top and bottom 1/3 of the circular sidewall of the cylinder are made of copper, which is electroplated with a thin layer of gold. Sandwiched in the middle of the circular sidewall are two pieces of a thermal insulating (curved) plate made of transparent Plexiglas.

control and relatively large Ra attainable for a given cell diameter, a natural question regarding this system is: to what extent can the experimental results and theoretical predictions for small aspect-ratio cells be applied to laterally large systems? This is an important question because one wants to understand which aspects of convection are universal and which depend on the details of spatial confinement [33]. Such an understanding is needed for a large number of practical problems, ranging from the thermal convection processes in buildings and metal production to natural convection occurred in the atmosphere and oceans and at geophysical and astrophysical scales, such as convection in the Earth's mantle and stars including the Sun [5].

Experimental efforts have been made recently to address this issue. Large upright cylindrical cells with diameter larger than 1 m were made in several laboratories [16,25,34], in order to increase the Rayleigh number Ra and to vary the aspect ratio $\Gamma = D/H$. Here we take a different approach to address this issue. Instead of using a large upright cylinder, we make a new convection cell of smaller size but with different geometry. The new cell has a shape of horizontal cylinder as shown in fig. 1. The top and bottom 1/3 of the circular sidewall of the cylinder are made of copper. Sandwiched in the middle of the circular sidewall are two pieces of a thermal insulating (curved) plate made of Plexiglas. Kadanoff [35] first proposed to build such a kind of cell in the hope that the circular cross-section of the horizontal cylinder could better accommodate the large-scale circulation.

We have carried out a systematic study of the convective flow in the horizontal cylinder filled with water. Global heat transport and local temperature and velocity measurements are made over varying Ra and spatial positions in the cylinders of different length. In this letter, we report key results of the experimental study focusing on the geometry dependence of the scaling laws in turbulent convection. Results obtained in the horizontal cylinder are compared with those obtained in the upright cylinder.

Apparatus and experimental methods. – The convection experiment is conducted in two horizontal cylindrical cells filled with water. The two cylindrical cells have the same inner diameter $D = 18.8$ cm but their lengths are different; one is $L = 9.4$ cm and the other is $L = 18.8$ cm. The corresponding aspect ratio ($\Gamma = L/D$) of the two cells is $\Gamma = 0.5$ and $\Gamma = 1$, respectively. Figure 1 shows the assembly of the horizontal convection cell. The top and bottom 1/3 of the circular sidewall of the cylinder are made of copper with a wall thickness of 0.5 cm. The surfaces of the conducting plates are electroplated with a thin layer of gold. Sandwiched in the middle of the circular sidewall are two pieces of a thermal insulating (curved) plate made of transparent Plexiglas. The two flat-end walls of the cell are made of the same transparent Plexiglas with a wall thickness of 2.3 cm. Two silicon rubber film heaters connected in parallel are sandwiched on the back side of the bottom 1/3 conducting plate to provide constant and uniform heating. The top 1/3 conducting plate is in contact with a cooling chamber consisting of many squarely winded water channels of 1 cm in width. These water channels are doubly winded with a channel separation of 0.5 cm, so that the incoming cooler fluid and the outgoing warmer fluid in adjacent channels can compensate with each other and provide uniform cooling on the top plate. A temperature-controlled circulator with a temperature stability of 0.01 °C is used to maintain the top-plate temperature. The entire cell is placed inside a thermostat box, whose temperature matches the mean temperature of the bulk fluid, which is fixed at ~ 30 °C.

The Rayleigh number for the horizontal cylinder is defined as $Ra = \alpha g \Delta T D^3/(\nu\kappa)$, where the cylinder diameter D is used as the cell height. In the experiment, the value of Ra is varied in the range $10^8 \lesssim Ra \lesssim 10^{10}$, and the Prandtl number is fixed at $Pr \simeq 5.4$. The temperature of each conducting plate is measured using 4 thermistors (Model 44006, Omega) of diameter 2.4 mm and time constant 1 s, which are embedded in the conducting plate. A digital multimeter is used to simultaneously measure the resistance value of the thermistors. The local temperature of the conducting fluid is measured using a waterproof thermistor (AB6E3-B05, Thermometrics) of diameter 0.3 mm and time constant 10 ms (in water). This thermistor is connected to an ac transformer bridge as a resistor arm and the other resistor arm is connected to a variable resistor to balance the bridge. The bridge is driven by a lock-in amplifier at a working frequency $f_0 \simeq 1$ kHz. The output signals are digitized by an A-to-D card at a sampling rate of 40 Hz. All the thermistors are calibrated individually with an accuracy of 5 mK. Typically, we take 8-h-long time series data (1.15×10^6 data points) at a fixed location for the statistical analysis of temperature fluctuations.

The vertical heat transport across the convection cell is measured by the dimensionless Nusselt number, $Nu = (P/S)/[k(\Delta T/D)]$, where P is the net input power to the convection cell and S $(= LD)$ is the cross-sectional area at the middle height of the cell. The net input flux P/S is normalized by the conductive heat transfer $k(\Delta T/D)$, where k is the thermal conductivity of water, D is the equivalent cell height (*i.e.*, the cylinder diameter), and ΔT is the temperature difference across the top and bottom conducting plates. The net input power P is calculated using the equation $P = P_t - P_b - P_s$, where P_t is the total electric input power to the heaters, P_b is the leakage power through the bottom plate, and P_s is the heat transfer through the side and end walls. The back of the bottom plate is wrapped with an insulating layer of rubber sheet (Insulflex) to reduce heat leakage. Two thermistors are placed across the rubber sheet to calculate the heat leakage power P_b. The side and end walls of the cell are covered with a layer of polystyrene foam of 15 mm in thickness. The heat transfer P_b is calculated using the known thermal conductivity of Plexiglas.

Local velocity measurements are conducted using a laser Doppler velocimetry (LDV) system (TSI Inc.) together with an argon-ion laser (Coherent Innova 90). The two flat-transparent-end walls are used as optical winders to admit the incident laser beams and observe the scattered light by the seed particles. A pair of laser beams from the LDV fiber optic transceiver is directed through the optic window and focused onto a single point inside the convection cell. The fiber optic transceiver has receiving optics to collect the scattered light in the backward direction and feeds it to a photomultiplier tube. The laser focusing spot has a cylindrically shaped probe volume of 1.31 mm in length and 0.09 mm in diameter. Monodispersed polymer latex spheres of 5.1 μm in diameter are used as seed particles. Because their density $(= 1.05\,\mathrm{g/cm^3})$ matches closely to that of water, the seed particles follow the local flow well.

Results and discussion. – Figure 2 shows the measured Nusselt number Nu as a function of Ra in the $\Gamma = 1$ (circles) and $\Gamma = 0.5$ (triangles) cells. The measured $Nu(Ra)$ curves can be well described by an effective power law $Nu = A_1 Ra^{\alpha}$. The fitted values of A_1 and α for both cells are given in table 1. The solid line shows an example of the power law fit to the triangles. A large number of heat transport measurements have been carried out in the $\Gamma = 1$ upright cylinder. These measurements were conducted in various convecting fluids with great precision and over a wide parameter range of Ra and Pr [1,7–16]. For comparison, we plot in fig. 2 a sample $Nu(Ra)$ curve obtained in the $\Gamma = 1$ upright cylinder [36], $Nu = 0.19Ra^{0.28}$ (dashed line). This example is chosen because the experiment used the same convecting fluid (water) and was conducted in a convection cell made of similar materials. Such a comparison can reduce the effect of possible systematic errors. It is seen from table 1 that the obtained values of α in the horizontal cylinders agree well with that for the upright cylinder. Figure 2 thus demonstrates that the Ra scaling of the Nusselt number in the horizontal cylinder remains unchanged. Evidently, the boundary layer dynamics, which determine the global heat transport, remain the same under different cell geometry.

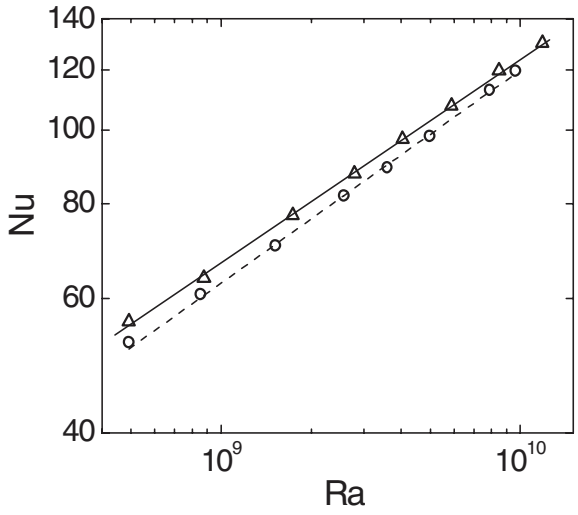

Fig. 2: Measured Nusselt number Nu as a function of Ra in the $\Gamma = 1$ (circles) and $\Gamma = 0.5$ (triangles) cells. The solid line is a power law fit to the triangles: $Nu = 0.25Ra^{0.27}$. The dashed line indicates the measured Nu in the $\Gamma = 1$ upright cylinder [36]: $Nu = 0.19Ra^{0.28}$.

From a systematic flow visualization study [37], we find that there also exists a large-scale circulation (LSC) across the horizontal cylinder. The rotation plane of LSC oscillates between the two long diagonal planes of the horizontal cell. Figure 3 shows the measured vertical velocity profile $U(r)$ at the mid-height of the $\Gamma = 1$ cell. The velocity measurements are made in one of the long diagonal planes and is along the radial distance r away from the cell center. The distance r is normalized by the diagonal distance r_0 $(= 13.3\,\mathrm{cm})$ from the cell center to the corner of the horizontal cell. It is seen that the flow in the rotation plane of LSC is like a flywheel with a zero mean velocity at the cell center. The mean vertical velocity increases linearly with the radial distance r in the bulk region of the flow. In the corner region of the horizontal cylinder, where thermal plumes accumulate, the mean vertical velocity increases more rapidly with r, because of the strong buoyancy forces exerted by the thermal plumes in the region. A similar flow structure was also observed in the $\Gamma = 1$ upright cylinders [17,18].

To study the Ra-dependence of the Reynolds number Re, we measure the horizontal velocity at $\sim$0.8 cm above the center of the bottom conducting plate. This is a symmetric point in the cell, which always stays in the rotation plane of LSC. When LSC oscillates between the two long diagonal planes of the horizontal cell, its

Table 1: Summary of the power law fits. The fits are all in the form: Quantity $= A_i \times Ra^{index}$, where $i = 1, 2, 3$ and index $= \alpha, \beta, \gamma$. References are given in parenthesis for the values of A_i and the indices, which are obtained in the upright cylinders.

Quantity	Horizontal cylinder $\Gamma = 1$	Horizontal cylinder $\Gamma = 0.5$	Upright cylinder $\Gamma = 1$
Nu	$A_1 = 0.20 \pm 0.02$	0.25 ± 0.02	0.19 ± 0.01
	$\alpha = 0.28 \pm 0.01$	0.27 ± 0.01	0.28 ± 0.06 [36]
Re	$A_2 = 0.10 \pm 0.01$	0.020 ± 0.003	0.075
	$\beta = 0.46 \pm 0.03$	0.55 ± 0.03	0.46 [38]
$\sigma/\Delta T$	$A_3 = 3.03 \pm 0.30$	82.1 ± 8.0	0.153
	$\gamma = -0.29 \pm 0.03$	-0.47 ± 0.04	-0.14 [26]

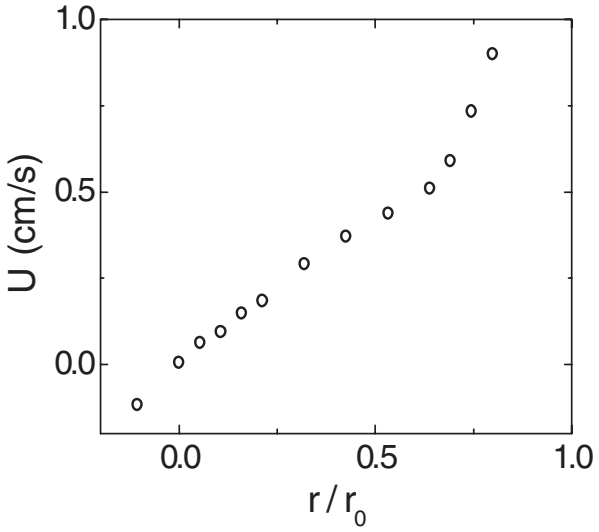

Fig. 3: Measured vertical velocity profile in the long diagonal plane of the $\Gamma = 1$ cell at $Ra = 4 \times 10^9$. The velocity measurements are made at the mid-height of the cell along the radial distance r away from the cell center with r_0 ($= 13.3$ cm) being the distance from the cell center to the corner of the horizontal cell.

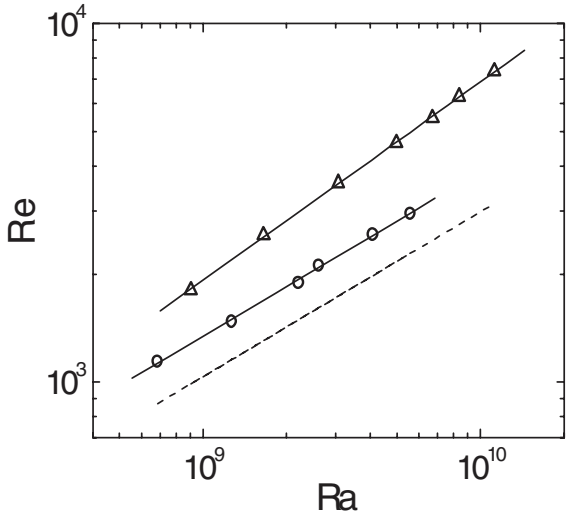

Fig. 4: Measured Reynolds number Re as a function of Ra in the $\Gamma = 1$ (circles) and $\Gamma = 0.5$ (triangles) cells. The upper solid line is a power law fit to the triangles, $Re = 0.02Ra^{0.55}$, and the lower solid line is a power law fit to the circles, $Re = 0.1Ra^{0.46}$. The dashed line indicates the measured Re in the $\Gamma = 1$ upright cylinder [38]: $Re = 0.075Ra^{0.46}$.

in-plane velocity U switches its direction from being positive to negative in the horizontal direction. Using the mean absolute value of the horizontal velocity U, we define the Reynolds number as $Re = UD/\nu$. Figure 4 shows the measured Re as a function of Ra in the $\Gamma = 1$ (circles) and $\Gamma = 0.5$ (triangles) cells. The measured $Re(Ra)$ curves can be well described by an effective power law $Re = A_2 Ra^{\beta}$. The fitted values of A_2 and β for both cells are given in table 1. The solid lines in fig. 4 show the power law fits to the circles and triangles, respectively.

For comparison, we also plot in fig. 4 the measured Re in the $\Gamma = 1$ upright cylinder [38], $Re = 0.075Ra^{0.46}$ (dashed line). The obtained value of β in the $\Gamma = 1$ horizontal cylinder agrees well with that obtained in the $\Gamma = 1$ upright cylinder. The measured value of β for the $\Gamma = 0.5$ horizontal cylinder shows a slightly larger deviation from the classical value of $\beta = 1/2$ for the free fall velocity [39]. Some of the deviations may be caused by a continuous evolution of the circulation path of LSC [40,41]. Figure 4 thus demonstrates that the Ra scaling of the Reynolds number in the horizontal cylinder remains approximately the same as that in the upright cylinder, insensitive to the change of cell geometry. Evidently, the buoyancy forces which drive the large-scale flow are independent of the cell geometry.

We now discuss the statistical properties of temperature fluctuations at the center of the $\Gamma = 1$ horizontal cell. Figure 5 shows the measured histograms, $H(\delta T)$, of the temperature fluctuation, δT, at two Rayleigh numbers: $Ra = 1.0 \times 10^9$ (squares) and $Ra = 8.3 \times 10^9$ (triangles). The histograms obtained at different values of Ra can all be brought into coincidence, once $H(\delta T)$ is normalized by its maximum value H_0 and δT is scaled by its rms value σ_T. Here the temperature fluctuation is defined as $\delta T = T - \langle T \rangle$ with $\langle T \rangle$ being the local mean temperature and $\sigma_T = \langle (T - \langle T \rangle)^2 \rangle^{1/2}$. Plots of $H(\delta T)/H_0$ *vs.* $\delta T/\sigma_T$ remain unchanged in the Ra range studied and only σ_T changes with Ra. The mean value of δT at the cell center is zero, and temperature fluctuations are symmetric relative to the zero mean. Over an amplitude range of almost six

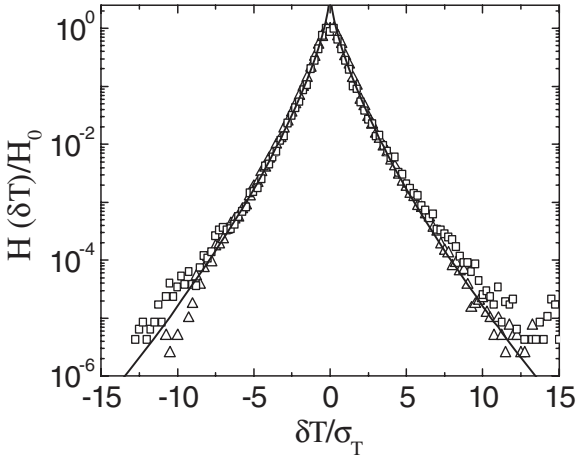

Fig. 5: Measured histogram, $H(\delta T)/H_0$, of the normalized temperature fluctuation, $\delta T/\sigma_T$, by its rms value σ_T. The measurements are made at the center of the $\Gamma = 1$ horizontal cell with $Ra = 1.0 \times 10^9$ (squares) and $Ra = 8.3 \times 10^9$ (triangles). The solid line shows the stretched exponential function, $H(\delta T)/H_0 = \exp[-b(\delta T/\sigma_T)^c]$, with the fitting values of $b = 2.59$ and $c = 0.68$.

decades, the measured histograms have a universal form, which can be well described by a stretched exponential function,

$$H(\delta T) = H_0 e^{-b(\delta T/\sigma_T)^c}. \quad (1)$$

The solid curve in fig. 5 shows the fit to the triangles with $b = 2.59 \pm 0.30$ and $c = 0.68 \pm 0.03$. Similar scaling behavior has also been observed in the $\Gamma = 1$ upright cylinders [1,26]. For the $\Gamma = 1$ upright cylinder, the measured $H(\delta T)$ has a simple exponential form with $c = 1$, whereas the measured $H(\delta T)$ in the horizontal cylinder has a slightly stretched exponential form with a c value close to but slightly less than unity.

While the cell shape appears not to affect the histogram of temperature fluctuations very much, it does affect the rms value of the temperature fluctuations. Figure 6 shows the normalized temperature rms value, $\sigma_T/\Delta T$, as a function of Ra. The measurements are made at the center of the $\Gamma = 1$ (circles) and $\Gamma = 0.5$ (triangles) cells. Here we find large differences in the Ra-dependence of $\sigma_T/\Delta T$ between the $\Gamma = 1$ and $\Gamma = 0.5$ cells. The measured $\sigma_T/\Delta T$ in both cells can also be described by an effective power law, $\sigma_T/\Delta T = A_3 Ra^\gamma$. The fitted values of A_3 and γ are given in table 1. The solid lines in fig. 6 show the power law fits to the circles and triangles, respectively.

For comparison, we also plot in fig. 6 the measured $\sigma_T/\Delta T$ in the $\Gamma = 1$ upright cylinder filled with water [26]: $\sigma_T/\Delta T = 0.153 Ra^{-0.14}$ (dashed line). A similar scaling result was also found in the $\Gamma = 1$ upright cylinder filled with low-temperature helium gas [1]. Evidently, the power law exponent γ varies considerably with the aspect ratio and the shape of the convection cell. In an early experiment [33], Daya and Ecke found that the value of γ for a square convection cell is different from that for an

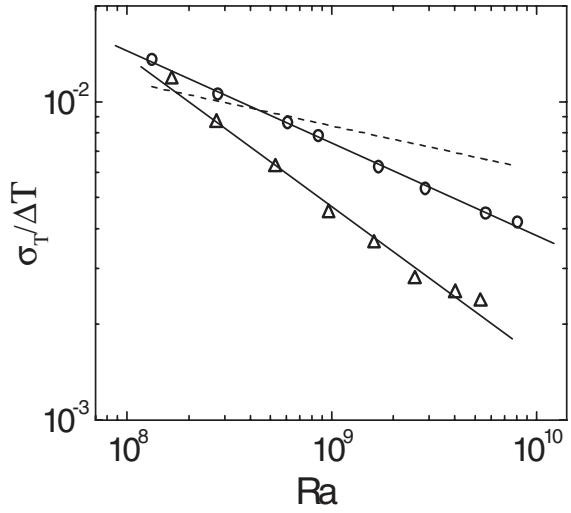

Fig. 6: Normalized temperature rms value, $\sigma_T/\Delta T$, as a function of Ra. The measurements are made at the center of the $\Gamma = 1$ (circles) and $\Gamma = 0.5$ (triangles) cells. The upper solid line is the power law fit to the circles, $\sigma_T/\Delta T = 3.03 Ra^{-0.29}$, and the lower solid line is the power law fit to the triangles, $\sigma_T/\Delta T = 82.1 Ra^{-0.47}$. The dashed line indicates the measured $\sigma_T/\Delta T$ in the $\Gamma = 1$ upright cylinder [26]: $\sigma_T/\Delta T = 0.153 Ra^{-0.14}$.

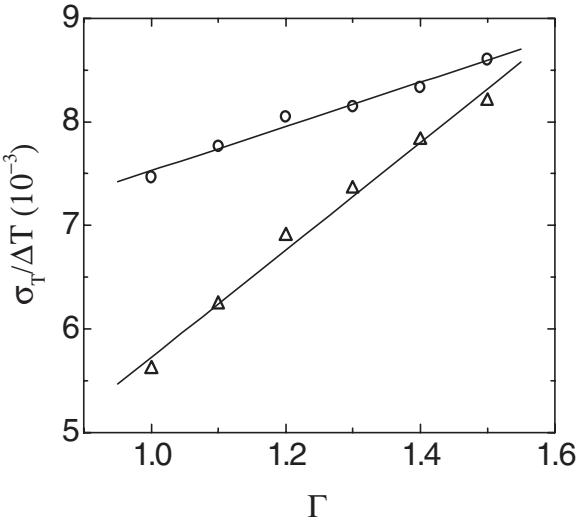

Fig. 7: Normalized temperature rms value, $\sigma_T/\Delta T$, as a function of the aspect ratio Γ. The measurements are made at the cell center with $Ra = 9.6 \times 10^8$ (circles) and 2.6×10^9 (triangles). The upper solid line is the linear fit to the circles, $\sigma_T/\Delta T = 5.4 \times 10^{-3} + 2.1 \times 10^{-3}\Gamma$, and the lower solid line is the linear fit to the triangles, $\sigma_T/\Delta T = 5.4 \times 10^{-4} + 5.2 \times 10^{-3}\Gamma$.

upright cylinder. The above results clearly reveal that local temperature fluctuations even at the cell center can still feel the boundary effect of the container.

To further investigate how $\sigma_T/\Delta T$ varies with the aspect ratio Γ, we install a mobile piston inside the cylinder, so that the working chamber of the horizontal cell has a variable length L (and hence Γ). Figure 7 shows the

measured $\sigma_T/\Delta T$ as a function of Γ. The measurements are made at the cell center with $Ra = 9.6 \times 10^8$ (circles) and 2.6×10^9 (triangles). In both cases, the measured $\sigma_T/\Delta T$ shows a linear dependence on Γ and the slope changes with Ra. The solid lines in fig. 7 show the linear fits to the circles and triangles, respectively. Figures 6 and 7 clearly reveal how the cell geometry influences the statistics of the local quantities, such as temperature fluctuations at the cell center.

In summary, we have carried out a systematic study of turbulent Rayleigh-Bénard convection in two horizontal cylindrical cells of different lengths filled with water. The measured Nusselt number $Nu(Ra)$ and the Reynolds number $Re(Ra)$ associated with the large-scale circulation are found to be insensitive to the change of cell geometry; their scaling over varying Rayleigh numbers remains unchanged. Evidently, the boundary layer dynamics, which determine the global heat transport, and the buoyancy forces which drive the large-scale flow remain the same under different cell geometry. However, the scaling behavior of the amplitude of local temperature fluctuations at the cell center is found to be strongly dependent on the aspect ratio and shape of the convection cell. These findings suggest that large-scale transport properties alone only provide a partial description of the convective flow and small-scale fluctuations depend more sensitively on the detailed structures of turbulent convection. It is a challenge for the turbulence theory to model the cell symmetry dependence of small-scale turbulent fluctuations. It is also a challenge for the experiment to further test whether this cell symmetry dependence will remain or not at even higher values of Ra and in much larger convection systems.

* * *

We have benefited from illuminating discussions with L. Kadanoff and D. Lohse. This work was supported by the Research Grants Council of Hong Kong SAR under Grant No. HKUST603208.

REFERENCES

[1] Castaing B., Gunaratne G., Heslot F., Kadanoff L., Libchaber A., Thomae S., Wu X.-Z., Zaleski S. and Zanetti G., *J. Fluid Mech.*, **204** (1989) 1.
[2] Siggia E., *Annu. Rev. Fluid Mech.*, **26** (1994) 137.
[3] Grossmann S. and Lohse D., *J. Fluid Mech.*, **407** (2000) 27.
[4] Kadanoff L. P., *Phys. Today*, **54**, issue No. 8 (2001) 34.
[5] Ahlers G., Grossmann S. and Lohse D., *Rev. Mod. Phys.*, **81** (2009) 503.
[6] Grossmann S. and Lohse D., *Phys. Fluids*, **16** (2004) 4462.
[7] Cioni S., Ciliberto S. and Sommeria J., *J. Fluid Mech.*, **335** (1997) 111.
[8] Glazier J. A., Segawa T., Naert A. and Sano M., *Nature*, **398** (1999) 307.
[9] Du Y.-B. and Tong P., *J. Fluid Mech.*, **407** (2000) 57.
[10] Chavanne X., Chill F., Chabaud B., Castaing B. and Hbral B., *Phys. Fluids*, **13** (2001) 1300.
[11] Niemela J. J., Skrbek L., Sreenivasan K. R. and Donnelly R. J., *Nature*, **404** (2000) 837.
[12] Niemela J. J. and Sreenivasan K. R., *J. Fluid Mech.*, **557** (2006) 411.
[13] Ahlers G. and Xu X.-C., *Phys. Rev. Lett.*, **86** (2001) 3320.
[14] Funfschilling D., Brown E., Nikolaenko A. and Ahlers G., *J. Fluid Mech.*, **536** (2005) 145.
[15] Xia X.-Q., Lam S. and Zhou S.-Q., *Phys. Rev. Lett.*, **88** (2002) 064501.
[16] Sun C., Ren L.-Y., Song H. and Xia K.-Q., *J. Fluid Mech.*, **542** (2005) 165.
[17] Qiu X.-L. and Tong P., *Phys. Rev. E*, **64** (2001) 036304.
[18] Sun C., Xia K.-Q. and Tong P., *Phys. Rev. E*, **72** (2005) 026302.
[19] Qiu X.-L. and Tong P., *Phys. Rev. Lett.*, **87** (2001) 094501.
[20] Zhou Q., Xi H.-D., Zhou S.-Q., Sun C. and Xia K.-Q., *J. Fluid Mech.*, **630** (2009) 367.
[21] Brown E. and Ahlers G., *J. Fluid Mech.*, **638** (2009) 383.
[22] Belmonte A., Tilgner A. and Libchaber A., *Phys. Rev. Lett.*, **70** (1993) 4067.
[23] Xin Y.-B., Xia K.-Q. and Tong P., *Phys. Rev. Lett.*, **77** (1996) 1266.
[24] Sun C., Cheung Y.-H. and Xia K.-Q., *J. Fluid Mech.*, **605** (2008) 79.
[25] du Puits R., Resagk C. and Thess A., *Phys. Rev. E*, **80** (2009) 036318.
[26] Du Y.-B. and Tong P., *Phys. Rev. E*, **63** (2001) 046303.
[27] Qiu X.-L., Shang X.-D., Tong P. and Xia K.-Q., *Phys. Fluids*, **16** (2004) 412.
[28] Shang X.-D., Qiu X.-L., Tong P. and Xia K.-Q., *Phys. Rev. Lett.*, **90** (2003) 074501; *Phys. Rev. E*, **70** (2004) 026308.
[29] Shang X.-D., Tong P. and Xia K.-Q., *Phys. Rev. Lett.*, **100** (2008) 244503.
[30] He X.-Z., Tong P. and Xia K.-Q., *Phys. Rev. Lett.*, **98** (2007) 144501.
[31] He X.-Z. and Tong P., *Phys. Rev. E*, **79** (2009) 026306.
[32] Lohse D. and Xia K.-Q., *Annu. Rev. Fluid Mech.*, **42** (2010) 335.
[33] Daya and Ecke , *Phys. Rev. Lett.*, **87** (2001) 184501.
[34] Ahlers1 G., Funfschilling D. and Bodenschatz E., *New J. Phys.*, **11** (2009) 123001.
[35] Kadanoff L. P., private communication.
[36] Lui S.-L. and Xia K.-Q., *Phys. Rev. E*, **57** (1998) 5494.
[37] Song H. and Tong P., in preparation.
[38] Qiu X.-L. and Tong P., *Phys. Rev. E*, **66** (2002) 026308.
[39] Sano M., Wu X.-Z. and Libchaber A., *Phys. Rev. A*, **40** (1989) 6421.
[40] Niemela J. J. *et al.*, *Europhys. Lett.*, **62** (2003) 829.
[41] Sun C. and Xia K.-Q., *Phys. Rev. E*, **72** (2005) 067302.